Korean J. Chem. Eng., 33(2), 638-648 (2016)
DOI: 10.1007/s11814-015-0170-3

pISSN: 0256-1115
eISSN: 1975-7220

Sorption of Cr(VI) by MgAl-NO_3 hydrotalcite in fixed-bed column: Experiments and prediction of breakthrough curves

Mohamed Khitous*,,***,†, Zineb Salem*, and Djamila Halliche****

*Laboratory of Process and Environmental Engineering LSGPI, Faculty of Mechanical and Process Engineering, University of Sciences and Technology, Houari Boumediene, BP 32 El-Allia, Bab Ezzouar, 16111 Algiers, Algeria
**Laboratory of Natural Gas Chemistry, Institute of Chemistry, University of Sciences and Technology, Houari Boumediene, BP 32 El-Allia, Bab Ezzouar, 16111 Algiers, Algeria
***Centre de Développement des Energies Renouvelables CDER, BP. 62 Route de l'observatoire, Bouzaréah 16340 Algiers, Algeria
(*Received 11 March 2015 • accepted 1 August 2015*)

Abstract−This study describes the sorption of Cr(VI) by MgAl-NO_3 hydrotalcite in a fixed-bed column. The sorbent was prepared via coprecipitation method and characterized by XRD, FTIR, BET surface area and pH_{zpc}. The effects of operating parameters such as bed height, flow rate and inlet concentration were investigated in continuous mode. As a result, the exhaustion time increased with the increase of bed height, decrease of flow rate and inlet concentration. A mathematical model based on the constant pattern theory and the Freundlich isotherm was applied to predict the experimental data, and to evaluate the model parameters of the fixed-bed column. The developed model describes well the breakthrough curves at various operating conditions. The calculated volumetric mass transfer coefficient K_La depends directly on these conditions. K_La increased with increasing flow rate and inlet concentration, while remained almost constant with varying bed height.

Keywords: Fixed-bed Column, Cr(VI), Breakthrough Curve, Model, Sorption

INTRODUCTION

Hexavalent chromium is widely used in various industries, such as electroplating, leather tanning, cement, mining and dyeing. Cr(VI), which causes severe environmental and public health issues [1], is highly mobile and is considered acutely toxic and mutagenic for most organisms; in humans its main effects are on skin, liver, kidney and respiratory organs, resulting in a variety of diseases such as dermatitis, hepatic and renal tubular necrosis, bronchitis and bronchogenic carcinoma [2,3]. The permissible limits of Cr(VI) in surface water and drinking water are 0.1 and 0.05 mg/L, respectively [4]. Therefore, it is necessary to treat the effluents and reduce the concentration of Cr(VI) to acceptable level before discharging them into aquatic environment.

Different techniques have been employed to remove Cr(VI) from wastewaters. Physicochemical treatments are commonly used because they are more economical than the electrochemical ones [5]. Among these techniques, sorption is one of the most effective physical processes for water treatment. It has been reported the use of zeolites [6], activated carbon [7], minerals [8], clays [9-11], chitosan [12] and biomass [13] as sorbent materials for Cr(VI).

Layered double hydroxides (LDHs), also known as hydrotalcite-like materials have received wide attention as an effective sorbent [14]. The general formula is $[M^{2+}_{1-x}\,M^{3+}_{x}\,(OH)_2]^{x+}\,(A^{n-})_{x/n}\,mH_2O$. M^{2+} and M^{3+} are divalent and trivalent cations, respectively; x is the M^{2+}/M^{3+} molar ratio and A^{n-} is the incorporated anion in the interlayer space along with water molecules for charge neutrality and structure stability [15]. LDHs are layered materials with hydroxide sheets, where a net positive charge is developed on the layer due to partial substitution of trivalent by divalent cations [16]. Due to the high charge density of the sheets and the exchangeability of the interlayer anions, LDHs have been used as sorbents to remove different harmful anions such as arsenate [17], phosphate [18], fluoride [19] and chromium [20].

Recently, extensive research has been undertaken to identify the ability of LDHs to remove Cr(VI) as well as to elucidate the sorption mechanism [20,21]. Several factors that affect the removal process, such as the structure of materials, solution pH, sorbent amount and thermal treatment were also investigated. However, they are limited to batch mode. This process is not convenient for application on an industrial scale, in which large volumes of wastewater are continuously generated. Thus, it is imperative to analyze continuous sorption data to provide valuable information for improving the design and removal operation from a wastewater treatment plant. In fact, a thorough literature survey indicated that uncalcined LDHs have not been used as sorbents to remove Cr(VI) in fixed bed column thus far.

Performance of continuous sorption process is described through the concept of breakthrough curve, i.e., the effluent concentration profile versus operating time. The breakthrough time and concentration profile are important characteristics to evaluate the dynamic behavior of a sorption column. The shape of the breakthrough

†To whom correspondence should be addressed.
E-mail: usthbkhitous@yahoo.fr

curve along the time depends on the column capacity with respect to the operating conditions. Therefore, the optimization of such separation process involves the modeling and prediction of experimental data. In fact, extensive studies in pilot plant scale can be avoided if the breakthrough curves may be reliably predicted using laboratory measurements [22].

Although, a variety of mathematical models have been developed to describe the performance of packed-bed columns, most of them are sophisticated and usually require the application of proper numerical methods [23,24]. However, the use of numerical solutions in such continuous process may show convergence problem, due to poor initialization and nonlinearity of the problem to be solved. Alternatively, several simple models have been proposed to predict breakthrough curve behavior, including the Thomas model [25], Clark model [26] and Bohart-Adams model [27]. However, although these models are suitable for the prediction of symmetrical breakthrough curves, they may be inadequate and fail to describe the performance of packed-bed columns with a complex sorption process. The modeling of breakthrough curves is challenging, due to the nonlinearity of equations used to describe the equilibrium, kinetic and mass transport phenomena involved in the sorption processes [28]. In fact, some authors have recognized that the development of breakthrough models for describing accurately the performance of packed-bed column is a difficult task [29].

Therefore, the scope of this study was to determine the sorption ability of prepared MgAl-NO_3 LDH to remove Cr(VI) from solutions using batch and continuous systems. The effects of design parameters such as column bed height, inlet concentration and flow rate were investigated using a laboratory scale fixed-bed column. In addition, a mathematical model based on the constant pattern theory and the Freundlich isotherm was developed to describe the continuous sorption of Cr(VI) by MgAl-NO_3 LDH. Finally, the experimental data obtained at various operating conditions were compared to the predicted breakthrough curves to evaluate the applicability of the model.

MATHEMATICAL MODEL

Several mathematical models were established for describing and analyzing the lab-scale column studies for the purpose of industrial applications [22,30,31].

We developed a mathematical model to predict the dynamic behavior of a fixed-bed column. The model is based on combining the constant-pattern wave approach theory and the Freundlich isotherm. The boundary condition at 50% of exhaustion ($C=C_0/2$ at $t=t_{1/2}$) is applied for symmetric breakthrough curves to solve the model equation. Modeling of breakthrough curves is achieved under the following assumptions: one-dimensional plug-flow, isothermal operation, absence of radial concentration gradient in the column, axial dispersion in the bed, spherical sorbent particles of homogeneous size, no chemical reaction occurs in the column, constant feed flow and bed porosity inside the column. The process of mass transfer between the solid and liquid phases is described by a linear driving force model that considers the hypothesis of instantaneous equilibrium.

The differential fluid phase mass balance for an element of sorption column is given as [23,32,33]:

$$U_0\frac{\partial C}{\partial Z}+\frac{\partial C}{\partial t}+\rho\frac{(1-\varepsilon)}{\varepsilon}\frac{\partial q}{\partial t}=D_L\frac{\partial^2 C}{\partial Z^2} \quad (1)$$

where U_0 (cm/min) is the interstitial velocity of the liquid, t (min) is the operating time, ε is the bed void fraction, Z (cm) is the distance from the inlet of the bed, ρ (g/cm^3) is the bed density, D_L (cm^2/min) is the axial dispersion coefficient, C (mg/L) and q (mg/g) are the concentrations of Cr(VI) in the liquid and solid phases, respectively.

As reported by Carberry and Wendel [34], the axial dispersion term in Eq. (1) may be negligible if the bed height exceeds fifty particle diameters; this condition is accomplished in the sorption of Cr(VI) by MgAl-NO_3 LDH. Therefore, Eq. (1) is reduced to a first-order hyperbolic equation and the governing equation becomes:

$$U_0\frac{\partial C}{\partial Z}+\frac{\partial C}{\partial t}+\rho\frac{(1-\varepsilon)}{\varepsilon}\frac{\partial q}{\partial t}=0 \quad (2)$$

Eq. (2) is subjected to the initial and boundary conditions:

q (Z, 0)=0 (initially clean sorbent)

C (Z, 0)=0

C (0, t)=C_0 (constant composition at bed entrance)

$$\left.\frac{\partial C(Z,t)}{\partial Z}\right|_{Z=H}=0$$

where H (cm) is the bed height.

The sorption rate can be described by the linear driving force model in terms of the overall liquid phase mass transfer coefficient [35]:

$$\rho\frac{\partial q}{\partial t}=\varepsilon K_L a(C-C_e) \quad (3)$$

where K_L (cm/min) is the overall liquid-phase mass transfer coefficient, a (cm^2/cm^3) is the contact area per unit volume of the bed, K_La (min^{-1}) is the volumetric mass transfer coefficient, C_e (mg/L) and q_e (mg/g) are the concentrations of Cr(VI) in the liquid and solid phases at equilibrium, respectively.

The correlation of Ranz and Marshall was selected to determine the overall liquid-phase mass transfer coefficient K_L [36], because it is applicable over a wide range of conditions and has widely applied to packed beds. The equation is given as:

$$Sh=2.0+0.6Sc^{1/3}Re^{1/2} \quad (4)$$

where Sh, Re and Sc are Sherwood, Reynolds and Schmidt numbers, respectively.

In this equation [37], $Re=\rho_L U_0 \varepsilon d_{pm}/\mu$, $Sc=\mu/(\rho_L D_m)$ and $Sh=K_L d_p/D_m$.

where ρ_L (g/cm^3) is the liquid density, μ (g/cm·s^{-1}) is the liquid viscosity, d_p (μm) is the particle diameter, D_m (cm^2/s) is the molecular diffusivity of Cr(VI) ions and d_{pm} (μm) is the mean particles diameter, which can be calculated by using the following equation [38]:

$$d_{pm}=\frac{1}{\sum x_i/d_i} \quad (5)$$

Table 1. Model parameters for prediction of breakthrough curves

Parameter	Value
ε Bed porosity	0.39
ρ Bed density (kg/m^3)	1460
ρ_L Liquid density (kg/m^3)	1000
μ Liquid viscosity (kg/m·s^{-1})	10^{-3}
D_m Molecular diffusivity (cm^2/s)	1.5 10^{-7} [40]
d_p Particle diameter (μm)	100
d_{pm} Mean particles diameter (μm)	206

where x_i is the mass fraction of particles with diameter d_i.

The contact area per unit volume of the bed (a) is calculated from Eq. (6) [39]:

$$a = \frac{6(1-\varepsilon)}{d_p} \tag{6}$$

The sorption isotherm related the liquid and solid phase concentration at equilibrium, C_e=f (q).

Two groups of model parameters can be recognized in the above equations: structural model parameters (d_p, ε and ρ) and transport model parameters (K_L, D_m, μ and a). In this study, the packed bed contains a mixture of sorbent and glass sand with a weight ratio of 10 : 90% in order to improve the penetration performance. Therefore, we can assume that glass sand is the only one that determines the flow rate of interstitial liquid. The apparent density of the bed was determined with a pycnometer, while the bed porosity was measured during the experiments. The physico-chemical characteristics of the bed and feed solution are listed in Table 1.

RESOLUTION METHOD

According to the constant-pattern wave approach theory [34], the mass balance equation may be put into a more concise form by using the method of combination of variables. Therefore, the liquid phase concentration can be expressed as a unique function of the adjusted time τ, defined as:

$$\tau = t - \frac{Z}{U_C} \tag{7}$$

where τ (min) is the relative time that represents the difference between the real time (from the start of the experiment) and the local liquid residence time, U_C (cm/min) is the concentration wave velocity.

Making the substitution of Eq. (7) into the governing equation, and after integration leads to:

$$\left(1-\frac{U_0}{U_C}\right)C + \frac{\rho(1-\varepsilon)}{\varepsilon}q = 0 \tag{8}$$

In the initial breakthrough zone, the amount of Cr(VI) introduced in the column is entirely retained in the bed. Hence, we can assume a rapid equilibrium between the liquid and solid phases. In this condition, the initial concentration in the solid phase q_0 can be used as an initial concentration for desorption tests. Therefore, the following condition, $q=q_0$ at $C=C_0$ is satisfied all the time.

Thus, we can make the following equation:

$$\left(1-\frac{U_0}{U_C}\right)C_0 + \frac{\rho(1-\varepsilon)}{\varepsilon}q_0 = 0 \tag{9}$$

where C_0 (mg/L) is the feed concentration of Cr(VI) in the liquid phase and q_0 (mg/g) is its associated concentration in the solid phase.

Combining Eqs. (8) and (9) leads to:

$$\frac{q}{q_0} = \frac{C}{C_0} \tag{10}$$

The sorption rate in terms of the adjusted time becomes:

$$\rho\frac{dq}{d\tau} = \varepsilon K_L a(C - C_e) \tag{11}$$

Combining Eqs. (10) and (11) gives:

$$\frac{\rho q_0}{C_0}\frac{dC}{d\tau} = \varepsilon K_L a[C - f(q_0 C/C_0)] \tag{12}$$

which can be rearranged and integrated with the following boundary condition, $C=C_0/2$ at $\tau=\tau_{1/2}$.

$$\int_{C_0/2}^{C}\frac{1}{C - f(q_0 C/C_0)}dC = \int_{\tau_{1/2}}^{\tau}\varepsilon K_L a\frac{C_0}{\rho q_0}d\tau \tag{13}$$

where $\tau_{1/2}$ is the adjusted time when the effluent concentration reaches half of the feed concentration.

Assuming a constant K_La and combining ($\tau - \tau_{1/2} = t - t_{1/2}$) in Eq. (13), the breakthrough curves at the top of column (Z=H) can be calculated by using the following equation:

$$t = t_{1/2} + \frac{\rho q_0}{\varepsilon K_L a C_0}\int_{C_0/2}^{C}\frac{1}{C - f(q_0 C/C_0)}dC \tag{14}$$

The sorption equilibrium is described by the Freundlich model:

$$C_e = \left(\frac{q}{K_{Fr}}\right)^n = f(q) \tag{15}$$

Combining Eqs. (10), (15) with Eq. (14) and assuming $x=C/C_0$, leads to:

$$t = t_{1/2} + \frac{\rho q_0}{\varepsilon K_L a C_0}\int_{0.5}^{x}\frac{1}{x - \frac{x^n}{C_0}\left(\frac{q_0}{K_{Fr}}\right)^n}dx \tag{16}$$

where x is the normalized effluent concentration.

Because q_0 is in equilibrium with C_0, therefore the following equation is also valid:

$$\frac{1}{C_0}\left(\frac{q_0}{K_{Fr}}\right)^n = 1 \tag{17}$$

Eq. (16) becomes:

$$t = t_{1/2} + \frac{\rho q_0}{\varepsilon K_L a C_0}\int_{0.5}^{x}\frac{1}{x - x^n}dx \tag{18}$$

With integration, we obtain:

$$\int_{0.5}^{x}\frac{1}{x - x^n}dx = \int_{0.5}^{x}\frac{1}{x}dx + \int_{0.5}^{x}\frac{x^{n-2}}{1 - x^{n-1}}dx \tag{19}$$

Combining Eq. (19) with Eq. (18) and integration leads to:

$$t = t_{1/2} + \frac{\rho q_0}{\varepsilon K_L a C_0}\left[\mathrm{Ln}2x - \frac{1}{n-1}\mathrm{Ln}\frac{1-x^{n-1}}{1-2^{1-n}}\right] \quad (20)$$

Eq. (20) represents a model of breakthrough curve using the Freundlich isotherm.

MATERIALS AND METHODS

1. Sorbent Preparation

MgAl-NO_3 LDH was prepared via co-precipitation method at constant pH. $Mg(NO_3)_2{\cdot}6H_2O$ and $Al(NO_3)_3{\cdot}9H_2O$ solutions were added dropwise into $NaNO_3$ solution. 50 mL of MgAl precursor solution containing 0.025 mol Mg^{2+} and 0.0125 mol Al^{3+} was added to 50 mL of anion solution containing 0.025 mol NO_3^-. The pH of precipitation was adjusted to 10 by adding 3.4 M NaOH solution under vigorous stirring. The obtained precipitate was aged at 60 °C in an oil bath shaker for 24 h, cooled and filtered. The precipitate was washed repeatedly with distilled water to reach a neutral pH and then dried at 80 °C for 24 h. Finally, the resulting solid was ground manually in a mortar and sieved to yield powder of 50-100 μm in diameter.

2. Sorbent Characterization

Powder X-ray diffraction (XRD) analysis identified the LDH phase using an XPERT-PR diffractometer, with CuKα radiation (λ=1.54060 Å) at 45 kV and 40 mA. Scanning diffraction angle was set at the speed of 0.06°/s. The BET surface area and average pore diameter were measured from the N_2 adsorption/desorption isotherms at 77 K by using Tri-Star II 3020 V1.03 Micromeritics surface area and pore size analyzer. Elemental chemical analysis was performed with an inductivity coupled plasma emission spectrometer for metal ions to determine the Mg/Al molar ratio of the LDH sample. 0.04 g of sample was dissolved in solution containing 15 mL of HNO_3 and 5 mL of HCl. Fourier transform infrared (FTIR) spectra of material before and after sorption were recorded by using an ALPHA Bruker FT-IR spectrometer over the 4,000-400 cm^{-1} wavenumber range.

The pH at the point of zero charge (pH_{zpc}) of the sorbent was determined using NaCl solutions at 0.1 and 0.05 M as inert electrolyte. The initial pH was adjusted from 2 to 13 by adding HNO_3 and NaOH solutions at 0.1 M. The experiments were performed on a thermostatic stirrer at 200 rpm and 20 °C for 2 h, by contacting 20 mg of LDH sample to 100 mL of each solution. Then, the suspensions were filtred and the final pH was measured. The pH_{zpc} was obtained through the plot of pH_{final} versus $pH_{initial}$ [41].

3. Stock Solution and Chromium Analysis

Chromium stock solution used for the experiments was prepared by dissolving accurately weighed K_2CrO_4 salt in distilled water to obtain a concentration of 500 mg/L. The stock solution was diluted with distilled water to obtain other concentrations. The solution pH was adjusted to the desired values by adding negligible volumes of HCl and NaOH solutions at 0.1 N. The concentration of Cr(VI) in solution was determined by using 1.5-Diphenyl carbazide (DPC) UV-visible spectrophotometry method at 540 nm [42].

4. Batch Experiments

The experiments were at room temperature in 100 mL bottles containing 50 mL of solution with a given dose of sorbent. The solution was stirred with a magnetic stirrer and the sorbent was separated by centrifugation at 1,200 rpm. The effects of operating parameters such as initial concentration, solution pH and sorbent amount were investigated by varying the studied parameter while keeping other parameters constant. All assays were in triplicate and only means values are presented.

The sorption capacity was determined from Eq. (21):

$$q_t = \frac{V(C_0 - C_t)}{m} \quad (21)$$

where C_0 and C_t (mg/L) are the concentrations initially and at time t, respectively; q_t (mg/g) is the amount of Cr(VI) sorbed at time t, m (g) is the sorbent mass and V (L) is the volume of solution.

5. Equilibrium Sorption Measurements and Modelling

Sorption isotherm data were generated by contacting 0.1 g of sorbent with Cr(VI) in aqueous solution. 50 mL of Cr(VI) solutions ranging from 5 to 200 mg/L were introduced in 100 mL bottles. The solutions were stirred for 2 h to ensure complete sorption equilibrium.

The equilibrium data were analyzed by the Langmuir and Freundlich models [43,44].

$$q_e = \frac{q_m K C_e}{1 + K C_e} \quad (22)$$

$$q_e = K_F C_e^{1/n} \quad (23)$$

where C_e (mg/L)and q_e (mg/g) are the concentrations of Cr(VI) in the liquid and solid phases at equilibrium, respectively. K (L/mg) is the Langmuir constant, q_m (mg/g) is the saturated sorption capacity of the sorbent, K_F and n are the Freundlich parameters. These parameters were determined using non-linear regression of experimental data according to Eqs. (22) and (23).

6. Column Study

Fig. 1 shows a schematic diagram of the setup for the continuous sorption study. The experiments were conducted in a laboratory scale Plexiglas column of 1.5 cm internal diameter and 20 cm length at 20 °C, where glass sand of 200 μm diameter and sorbent were mixed with a weight ratio of 90 : 10% to improve the penetration performance. Glass sand was thoroughly washed by distilled water and dried at 100 °C for 24 h. The sorbent bed was supported and closed by glass beads of 800 μm diameter to ensure a

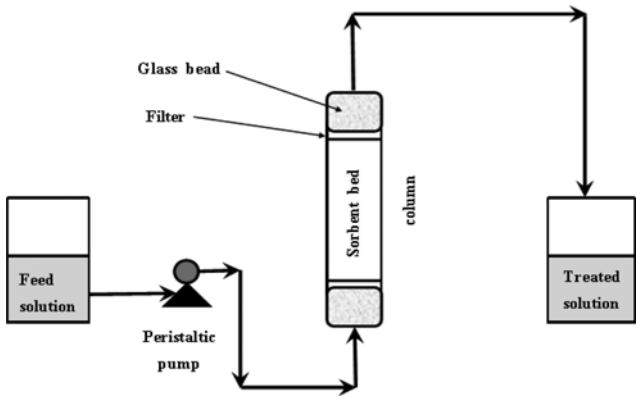

Fig. 1. Experimental system for column sorption.

good liquid distribution. A filter was also placed in the bottom and top of the column to avoid any loss of sorbent (Fig. 1).

The solution was fed through the column by using a peristaltic pump in an up-flow direction to avoid channeling of solution and compaction. The effluent samples were collected from the top of column at defined time intervals and analyzed for the remaining Cr(VI) concentration. The flow to the column was continued until the outlet concentration approached the inlet concentration. The column experiments were carried out as a function of flow rate, inlet concentration and bed height.

The chromium uptake in the column q (mg/g) is calculated from the area under the breakthrough curve by the following equation:

$$q = \frac{Q}{1000\ m}\left(C_0 t_s - \int_0^{t_s} C dt\right) \quad (24)$$

where C_0 and C (mg/L) are the initial and effluent concentrations at time t, respectively. t_s (min) is the exhaustion time, Q (mL/min) is the flow rate and m (g) is the mass of sorbent.

RESULTS AND DISCUSSION

1. Sorbent Characterization

From Fig. 2, it appears clearly that the XRD pattern of the sample has sharp and symmetric peaks at lower 2θ as (003) and (006), which are characteristic of the hydrotalcite-like compounds with a high degree of crystallinity. The pattern is indexed to a hexagonal cell [45]. No other phase is observed in the XRD pattern. The basal reflections $00l$ at low angles (11°, 2θ) correspond to the interlayer distance. The (110) reflection appears at high angles (61°, 2θ). The lattice parameters are estimated as $c = l \times d_{00l}$; $a = 2 \times d_{110}$ (Table 2). The results agree well with those reported by Srinivasa et al. [46], who suggest that a distance of around 8.9 Å is evocative of high interlayer spacing with a thickness of 2-3 atoms.

From Table 2, the resultant Mg/Al molar ratio of the sample was determined to be 1.97, showing good agreement with the initial value of the starting solutions. Therefore, MgAl-NO_3 LDH with Mg/Al molar ratio of 2 was successfully prepared. The surface area of MgAl-NO_3 LDH is very low (5.70 m^2/g). The result agrees with that reported by Wang et al. [47]. They have reported a low surface area (<9 m^2/g) for LDHs with NO_3^- as interlayer anion.

The FTIR spectra of MgAl-NO_3 LDH and its corresponding sample after sorption are shown in Fig. 3. The intense broad band observed at around 3,500-3,250 cm^{-1} associated with stretching vibration of O-H bond in the brucite-like layers $Mg(OH)_2$ and $Al(OH)_3$ [48,49]. The band at about 1,643 cm^{-1} can be assigned to the deformation vibration of water molecules in the interlayer domain [50]. The bands at 540-650 cm^{-1} can be due to the vibration of Al-O and Mg-O groups in the layers. The characteristic sharp absorption band at about 1,380 cm^{-1} is associated with the antisymmetric stretching mode of NO_3^- [51].

By comparison between the FTIR spectra of the sorbent before and after sorption, we can see that the solid remained the same characteristic bands, but their intensity was significantly reduced. This indicates that the solid maintains its chemical structure and anion-exchange reaction occurs between the solid and solution. As reported by Nakamoto [52], the characteristic band of free chromate appeared at 890 cm^{-1}, but it shifted towards the lower frequency slightly at about 878 cm^{-1}. This indicates that the Cr-O band for Cr-sorbent is weaker than that for free chromate [53].

The pH_{zpc} of MgAl-NO_3 LDH is around 7.8 as revealed by crossing point of the curves (Fig. 4), indicating an amphoteric surface, which is positively charged at pH lower than 7.8 while negatively charged when pH is higher than 7.8. Therefore, in addition to the main anion-exchange mechanism, there is electrostatic attraction between chromate ions and electropositive surface of LDH since the solution pH was below the pH_{zpc} of sorbent.

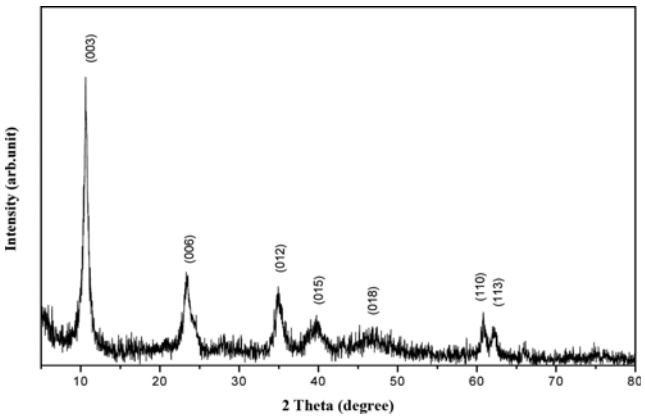

Fig. 2. XRD pattern of MgAl-NO_3 LDH (molar ratio, R=2).

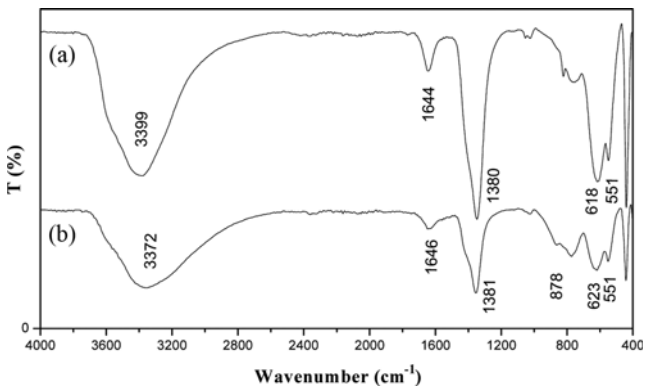

Fig. 3. FTIR spectra of MgAl-NO_3 LDH: (a) before and (b) after sorption.

Table 2. Characterization of MgAl-NO_3 LDH

Mg/Al molar ratio		BET surface area (m^2/g)	Average pore diameter (nm)	Cell parameters			
Synthesis solution	Obtained sample			d_{003} (Å)	d_{110} (Å)	a (Å)	c (Å)
2	1.97	5.70	10.54	8.369	1.524	3.048	25.11

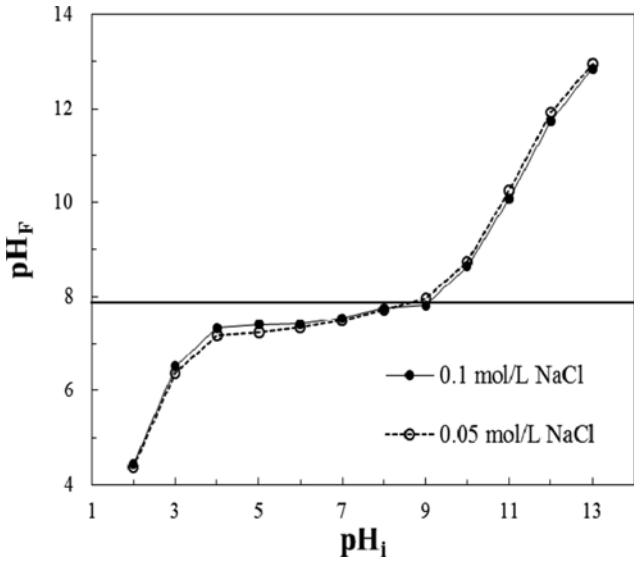

Fig. 4. pH_{final} as a function of $pH_{initial}$ for MgAl-NO_3 LDH (T=20 °C, m=0.05 g and V_{NaCl}=250 mL).

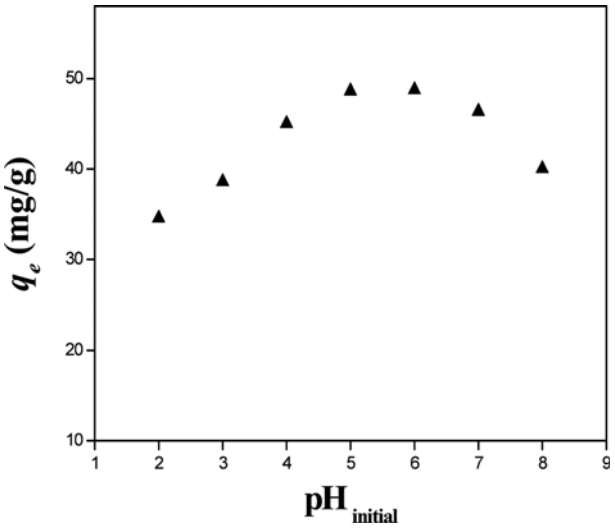

Fig. 5. Effect of solution pH for Cr(VI) removal using MgAl-NO_3 LDH (C_0=100 mg/L, m=2 g/L and T=20 °C).

2. Batch Study

2-1. Effect of Solution pH

The effect of solution pH was determined at pH values ranging from 2 to 8, initial concentration of 100 mg/L and sorbent dose of 2 g/L (Fig. 5). The solutions were stirred for a period of 2 h to allow sufficient time for sorption equilibrium.

Fig. 5 shows that the Cr(VI) removal onto MgAl-NO_3 LDH is pH dependent. The sorption capacity increased as the pH increased from 2 to 6, then decreased with increasing pH from 6 to 8. The high sorption capacity was obtained at solution pH of 5 and 6 (48 mg/g), which suggests the existence of an optimum pH for efficient removal of Cr(VI) ions.

In acid solutions, the surface of MgAl-NO_3 LDH is protonated and therefore acquires positive charges. The degree of protonation reduces with the pH increase, resulting in fewer positive charges to combine Cr(VI) from aqueous solution. However, under strongly acidic conditions (pH=3), low metal ion uptake is observed. This behavior can be explained by the dissolution of sorbent at very low pH.

In an alkaline pH condition (pH=8), the sorption capacity decreased compared with that obtained at pH ranging from 4 to 7. This is due to the charge reduction on the LDH surface because of the interaction with hydroxyl groups in solution. Therefore, the optimal pH was selected as 6 for the removal of Cr(VI) by MgAl-NO_3 LDH.

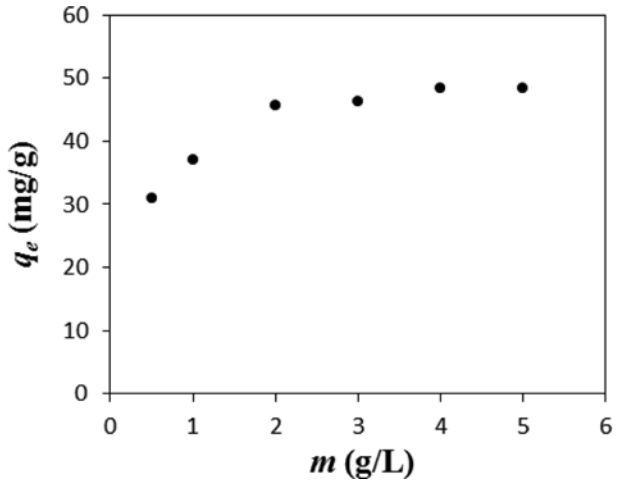

Fig. 6. Effect of sorbent dosage for Cr(VI) removal using MgAl-NO_3 LDH (pH=6, C_0=100 mg/L and T=20 °C).

2-2. Effect of Sorbent Dosage

The effect of sorbent dosage was investigated at various sorbent amounts ranging from 0.5 to 5 g/L. The concentration of Cr(VI) and solution pH were kept constant at 100 mg/L and 6, respectively (Fig. 6).

The sorption capacity increased with increasing sorbent dosage from 0.5 g/L (30.84 mg/g) to 2.0 g/L (45.72 mg/g) (Fig. 6). This is due to the increase of sorbent surface area and availability of the exchangeable sites at high sorbent concentration, offering more contact surface for Cr(VI) sorption. This behavior can be explained to the increase of the vacant sorption sites with more sorbent existing in solution [54]. It appears also that the sorption capacity remains almost constant as the sorbent dosage increased from 2 to 5 g/L. Therefore, this value was selected as an optimal sorbent dosage for batch experiments.

2-3. Effect of Initial Concentration

The effect of initial concentration on the removal of Cr(VI) by Mg-Al-NO_3 LDH was investigated at various concentrations ranging from 5 to 200 mg/L. The results are shown in Fig. 7.

Sorption was rapid in the first step, at the beginning up to 10 min and then slowed considerably till a saturation level was reached at 30 min. The initial rapid phase may be due to greater number of sorption sites available for the sorption of Cr(VI) ions. After 30 min, although the sorption capacity has a slight increase with increasing the contact time, it remains almost constant, meaning that the sorption equilibrium of Cr(VI) is reached.

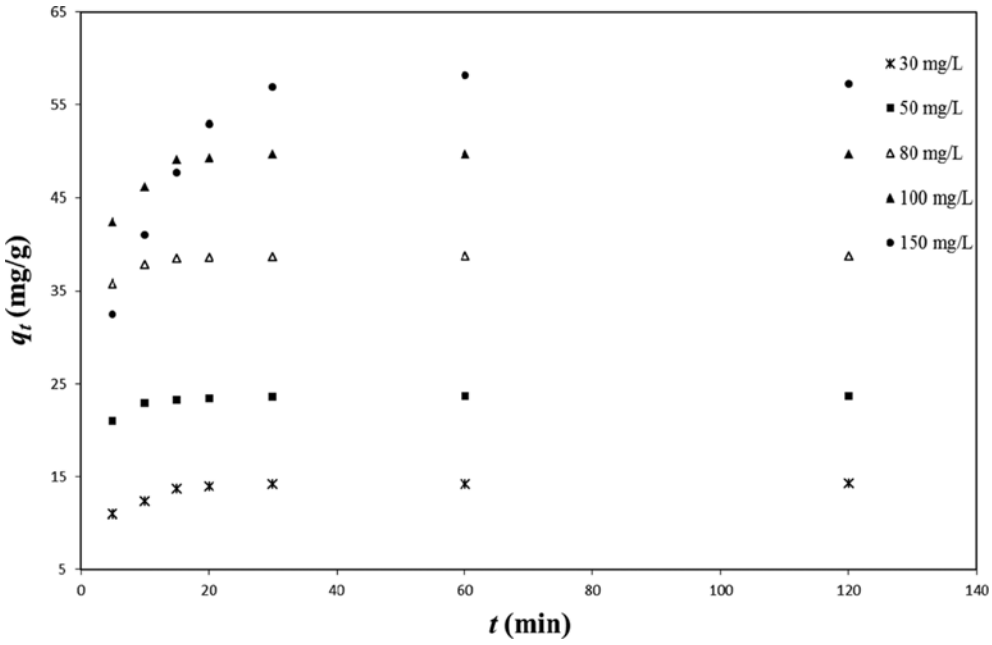

Fig. 7. Effect of initial concentration for Cr(VI) removal using MgAl-NO_3 LDH (pH=6, m=2 g/L and T=20 °C).

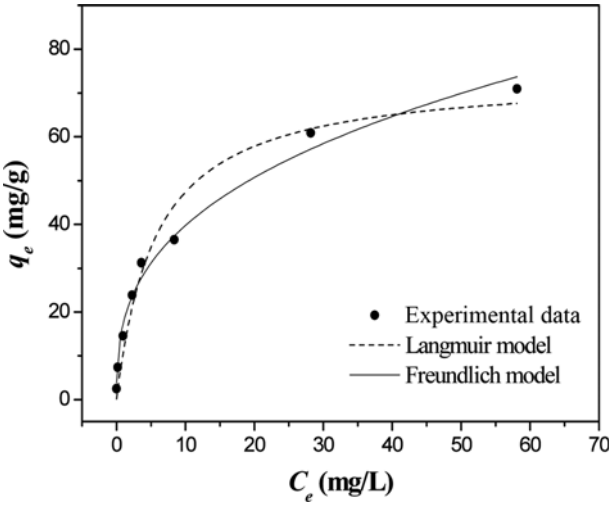

Fig. 8. Experimental and predicted sorption isotherms of Cr(VI) onto MgAl-NO_3 LDH.

3. Sorption Isotherm

The sorption isotherm of Cr(VI) onto MgAl-NO_3 LDH is shown in Fig. 8. According to the classification of Giles et al. [55], the sorption isotherm is H-type, indicating a high affinity between the sorbent and Cr(VI) so that it is almost completely sorbed from dilute solution.

The results obtained in Table 3 indicate that the Langmuir model is not as adequate as the Freundlich model (R^2=0.98). According to McKay et al. [56], the n values between 2 and 10 represent a good sorption. For Langmuir model, the relationship between the sorbed amount and its equilibrium concentration in the solution is adequately described. The maximum capacity q_m calculated by the Langmuir isotherm is close to that obtained at equilibrium (74.07 mg/g).

Table 3. Isotherm model parameters for Cr(VI) sorption by MgAl-NO_3 LDH

Isotherm model	Parameter	Value
Langmuir	K (L/mg)	0.18
	q_m (mg/g)	74.07
	R^2	0.953
Freundlich	n	2.85
	K_F	17.75
	R^2	0.986

4. Prediction of Breakthrough Curves

To investigate the sorption behavior of Cr(VI) by MgAl-NO_3 LDH in a fixed-bed column, the experiments were conducted as a function of flow rate, bed height and inlet concentration. The solution pH was kept as constant at optimal value of 6 obtained from batch study. The shapes of breakthrough curves obtained at various operating conditions were compared using a plot of dimensionless concentration C/C_0 versus time, as shown in Figs. (9), (10) and (11).

The applicability of Eq. (20) is justified by the linear plot, as shown in Fig. 12 (other results are not shown here). The results indicate a good applicability of the model with experimental data in the mass transfer zone ($0.05<C/C_0<0.95$). The values of $t_{1/2}$ and K_La were determined from the plots of [Ln 2x−1/(n−1) Ln[(1−x^{n-1})/(1−2^{1-n})] versus time according to Eq. (20). The results obtained in Table 4 show that the predicted parameters agree well with experimental ones obtained at various operating conditions.

Figs. (9), (10) and (10) show a good agreement between model and experimental data at various conditions. Therefore, the model describes sufficiently the continuous sorption of Cr(VI) by MgAl-NO_3 LDH.

4-1. Effect of Inlet Concentration

The effect of inlet concentration was investigated at various con-

Table 4. Experimental and predicted parameters for Cr(VI) sorption on MgAl-NO_3 LDH in fixed-bed column

C_0 (mg/L)	H (cm)	Q (mL/min)	t_p (min)	t_s (min)	q (mg/g)	K_La (min^{-1})	$t_{1/2}$ (min)		R^2
							Exp	Model	
30			160	290	66.93	269.51	220	220.75	0.990
80	3.5	10	70	160	84.90	291.25	100	100.17	0.973
100			55	125	88.83	301.84	90	88.28	0.994
	2		25	130	66.82	275.91	75	74.64	0.990
50	3.5	10	115	220	82.95	272.32	170	169.90	0.994
	5		150	260	87.91	267.58	210	210.47	0.991
50	3.5	5	180	310	86.05	241.04	250	249.56	0.998
		20	30	120	70.83	331.31	70	70.12	0.996

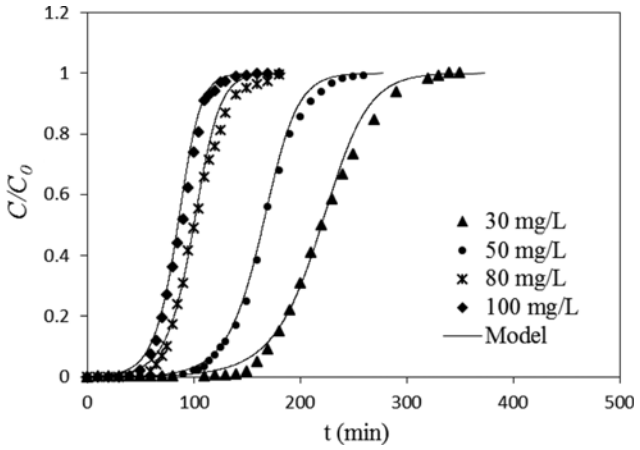

Fig. 9. Experimental and predicted breakthrough curves for Cr(VI) sorption by MgAl-NO_3 LDH at different inlet concentrations (Q=10 mL/min, H=3.5 cm and pH=6).

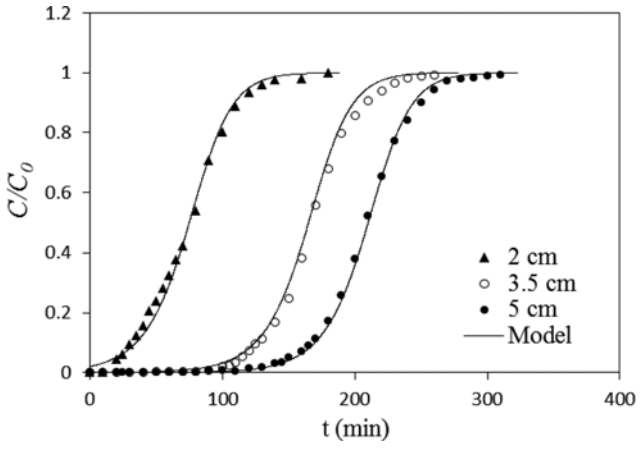

Fig. 10. Experimental and predicted breakthrough curves for Cr(VI) sorption by MgAl-NO_3 LDH at different bed heights (Q= 10 mL/min, C_0=50 mg/L and pH=6).

centrations ranging from 30 to 100 mg/L, at constant bed height and flow rate of 3.5 cm and 10 mL/min, respectively. The results are shown in Fig. 9.

From Table 4, the breakthrough time decreased from 160 min to 55 min as the concentration of Cr(VI) increased from 30 to 100 mg/L. This can be attributed to the fact that the sorption sites on MgAl-NO_3 LDH are rapidly filled with Cr(VI) ions at high concentrations, resulting in quick exhaustion of the bed and low uptake of Cr(VI).

The sorption capacity increased from 66.93 to 88.83 mg/g with increasing inlet concentration from 30 to 100 mg/L (Table 4), which can be due to the increase of driving force for the mass transfer process at high concentration. Therefore, high amount of Cr(VI) can be sorbed by MgAl-NO_3 LDH. However, based on the Cr(VI) removal efficiency, 50 mg/L was found to be the optimal inlet concentration.

As shown in Table 4, $t_{1/2}$ decreased with increasing inlet concentration while K_La increased slightly. This means that the breakthrough curve is steeper at high concentrations. It is likely that the driving force of mass-transfer in the liquid film is enhanced when C_0 increased. Lin et al. [57] found a similar tendency during the column sorption of acid dye onto pristine and acid-activated clays.

4-2. Effect of Bed Height

The effect of bed height on the column performance was studied at various bed heights of 2, 3.5 and 5 cm, at constant flow rate and inlet concentration of 10 mL/min and 50 mg/L, respectively. The breakthrough curves obtained at various bed heights are shown in Fig. 10.

From Table 4, the breakthrough time increased from 25 to 135 min as the bed height increased from 2 to 5 cm, respectively. The breakthrough curves become steeper with the decrease in bed height, resulting in early exhaustion of the bed. At high bed height, Cr(VI) ions have enough time to contact with sorbent, resulting in longer exhaustion time and high removal. The sorption capacity increased from 66.82 to 87.91 mg/g with increasing bed height from 2 to 5 cm, respectively. However, there is a slight increase in sorption capacity when the bed height increased from 3.5 to 5 cm. Therefore, the optimum bed height was selected at 3.5 cm for continuous sorption of Cr(VI). The obtained results are found to be similar to those reported by Lim [58] and Meng [59].

The values of K_La decreased slightly as the bed height increased, due to the tortuosity increasing and velocity variation in the bed. Moreover, the $t_{1/2}$ values are roughly proportional to the bed height. On the other hand, increasing bed height has a little effect on the K_La values. This behavior agrees with previous results for the sorption of phenols onto surfactant-modified montmorillonite in column systems [60].

4-3. Effect of Flow Rate

The effect of flow rate was investigated at flow rates ranging from

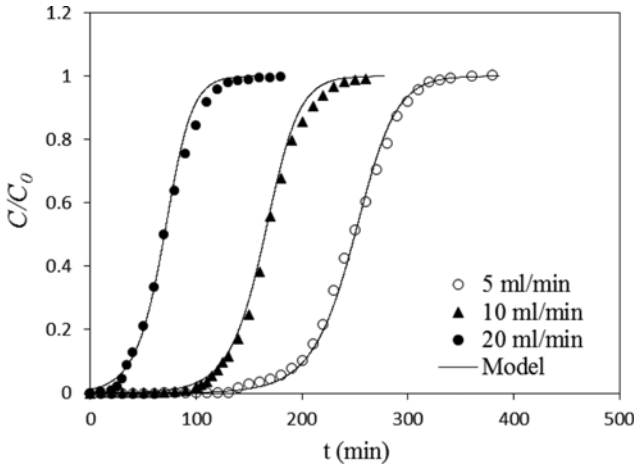

Fig. 11. Experimental and predicted breakthrough curves for Cr(VI) sorption by MgAl-NO_3 LDH at different flow rates (H=3.5 cm, C_0=50 mg/L and pH=6).

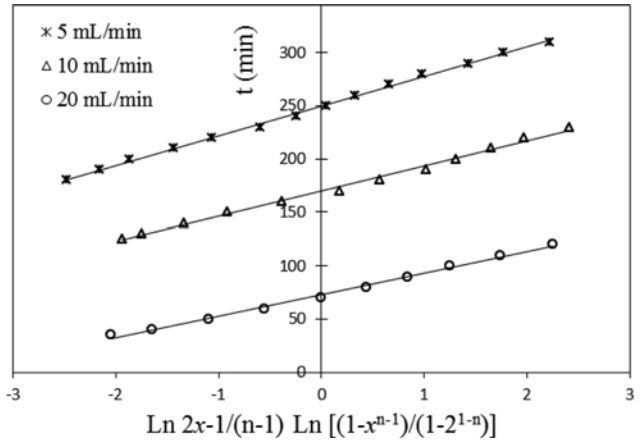

Fig. 12. Validity of the model for Cr(VI) removal by MgAl-NO_3 LDH at various flow rates (H=3.5 cm, C_0=50 mg/L and pH=6).

5 to 20 mL/min. The initial concentration and bed height were kept constant at 50 mg/L and 3.5 cm, respectively. The breakthrough curves obtained at various flow rates are shown in Fig. 11.

As expected, an increase in flow rate produced a reduction in breakthrough and exhaustion times. Consequently, the breakthrough curves became steeper with a shorter mass transfer zone, which can be explained by insufficient residence time for Cr(VI) ions in the column to progress mass transfer and removing from the solution. In addition, the sorption capacity slightly decreased from 86.05 to 70.83 mg/g with increasing flow rate from 5 to 20 mL/min, respectively (Table 4). Therefore, low flow rates lead to more efficient interactions between the sorbent and Cr(VI) ions. Similar results were also found by Shao [61] and Auta [62].

The influence of flow rate on the $t_{1/2}$ and K_La values is shown in Fig. 13. The results indicate a good linear dependence: $t_{1/2}$ decreased while K_La increased with increasing flow rate, which agrees with Chern and Chien [63] that K_La varied linearly with the flow rate. Moreover, the increase of flow rate provides a decrease of the external mass transfer resistance, consequently an increase in the overall mass transfer coefficient and mass transfer flux.

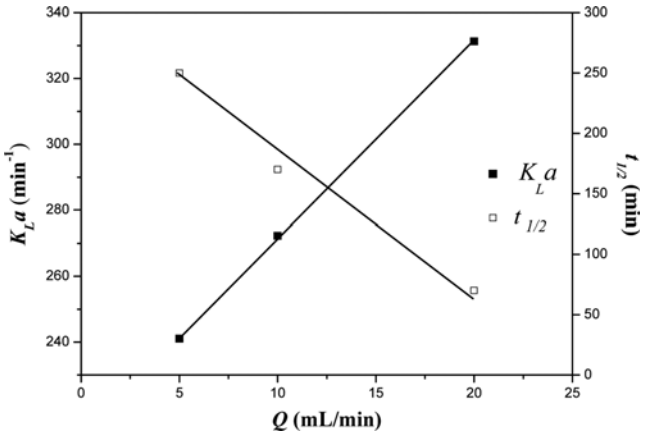

Fig. 13. Effect of flow rate on the volumetric mass transfer coefficients (H=3.5 cm, C_0=50 mg/L and pH=6).

CONCLUSION

$MgAl-NO_3$ layered double hydroxide was prepared via co-precipitation method and used as sorbent to remove Cr(VI) in fixed-bed column. The column experiments were carried out as a function of bed height, flow rate and inlet concentration. The continuous flow sorption of Cr(VI) is dependent on these parameters. The optimum conditions were achieved at 3.5 cm, 10 mL/min and 50 mg/L, respectively.

A mathematical model based on the constant pattern theory, linear driving force (LDF) model and the Freundlich isotherm was developed and applied to predict the experimental data obtained at various operating conditions. The developed model accurately describes the breakthrough curves. Two important parameters can be determined from the model, which are the time required for 50% breakthrough ($t_{1/2}$) and the volumetric mass transfer coefficient (K_La). They are related directly to the operating conditions. K_La increased with increasing flow rate and inlet concentration while $t_{1/2}$ decreased. $t_{1/2}$ is proportional to the bed height and K_La remains identical. These parameters can be used for the scale up of industrial processes.

NOMENCLATURE

a : contact area per unit volume of the bed [cm^2/cm^3]
C : sorbate concentration in the liquid phase [mg/L]
C_o : inlet concentration of sorbate in the liquid phase [mg/L]
C_e : sorbate concentration in the liquid phase at equilibrium [mg/L]
d_p : particle diameter [μm]
d_{pm} : mean particles diameter [μm]
D_m : molecular diffusivity of Cr(VI) ions [cm^2/s]
D_L : axial dispersion coefficient [cm^2/min]
H : bed height [cm]
K : Langmuir equilibrium constant [L/mg]
K_F and n : Freundlich constants
K_L : overall liquid-phase mass transfer coefficient [cm/min]

K_La : volumetric mass transfer coefficient [min^{-1}]
m : mass of sorbent [g]
Q : flow rate [mL/min]
q : sorbate concentration in the solid phase at time t [mg/g]
q_e : sorbate concentration in the solid phase at equilibrium [mg/g]
q_0 : sorbate concentration in the solid phase in equilibrium with C_o [mg/g]
q_m : maximum capacity calculated by Langmuir isotherm [mg/g]
Re : Reynolds number
Sc : Schmidt number
Sh : Sherwood number
t : operating time [min]
T : temperature [K]
$t_{1/2}$: time required for 50% sorbate breakthrough [min]
t_p : breakthrough time [min]
t_s : exhaustion time [min]
U_0 : interstitial velocity of fluid [cm/min]
U_C : velocity of the concentration wave [cm/min]
V : volume of solution [L]
W : shaking speed [rpm]
x : normalized effluent concentration
x_i : mass fraction of particles
Z : distance from the inlet of the bed [cm]
ε : bed void fraction
ρ : bed density [g/cm^3]
ρ_L : fluid density [g/cm^3]
μ : fluid viscosity [$g/cm \cdot s^{-1}$]
τ : adjusted time [min]
$\tau_{1/2}$: adjusted time when the effluent concentration reaches half of the feed concentration [min]

REFERENCES

1. E. Demirbas, M. Kobya, E. Senturk and T. Ozkan, *Water SA*, **30**, 533 (2004).
2. R. A. Goyer and M. A. Mehlman, *Advances in Modern Toxicology: Toxicology of Trace Elements*, John Wiley & Sons, New York (1977).
3. B. L. Carson, H. V. Ellis and J. L. McCann, *Toxicology and Biological Monitoring of Metals in Humans*, Lewis Publishers, Chelsea, Michigan (1986).
4. Environmental Protection Agency (EPA), Cincinnati, Ohio, Environmental pollution control alternatives: Drinking Water Treatment for Small Communities, EPA/625/5-90/025, California (1990).
5. W. J. McLay and F. P. Reinhard, *Met. Finish.*, **98**, 817 (2000).
6. B. A. Shah, C. B. Mistry and A. V. Shah, *Micropor. Mesopor. Mater.*, **196**, 223 (2014).
7. W. Daoud, T. Ebadi and A. Fahimifar, *Korean J. Chem. Eng.*, **32**(6), 1119 (2015).
8. S. A. Idris, K. M. Alotaibi, T. A. Peshkur, P. Anderson, M. Morris and L. T. Gibson, *Micropor. Mesopor. Mater.*, **165**, 99 (2013).
9. Q. Liu, B. Yang, L. Zhang and R. Huang, *Korean. J. Chem. Eng.*, **32**(7), 1314 (2015).
10. T. Kameda, E. Kondo and T. Yoshioka, *Sep. Purif. Technol.*, **122**, 12 (2014).
11. H. Fida, S. Guo and G. Zhang, *J. Colloid Interface Sci.*, **442**, 30 (2015).
12. L. Sun, Z. Yuan, W. Gong, L. Zhang, Z. Xu, G. Su and D. Han, *Appl. Surf. Sci.*, **328**, 606 (2015).
13. M. Salman, M. Athar, U. Farooq, H. Nazir, A. Noor and S. Nazir, *Korean J. Chem. Eng.*, **30**(6), 1257 (2013).
14. K. H. Goh, T. T. Lim and Z. L. Dong, *Water Res.*, **42**, 1343 (2008).
15. A. Ookubo, K. Ooi and H. Hayashi, *Langmuir*, **9**, 1418 (1993).
16. K. Xing, H. Z. Wang, L. G. Guo, W. D. Song and Z. P. Zhao, *Colloid Surf., A.*, **328**, 15 (2008).
17. S. L. Wang, C. H. Liu, M. K. Wang, Y. H. Chung and P. N. Chiang, *Appl. Clay. Sci.*, **43**, 79 (2009).
18. K. Yang, L. Yan, Y. Yang, S. Yu, R. Shan, H. Yu, B. Zhu and B. Du, *Sep. Purif. Technol.*, **124**, 36 (2014).
19. P. Koilraj and S. Kannan, *Chem. Eng. J.*, **234**, 406 (2013).
20. T. Hongo, H. Wakasa and A. Yamazaki, *Mater. Sci-Poland.*, **29**, 86 (2011).
21. V. Srinivasa, P. Prasanna and K. Vishnu, *Solid State Sci.*, **10**, 260 (2008).
22. R. Tovar-Gómez, M. R. Moreno-Virgen, J. A. Dena-Aguilar, V. Hernández-Montoya, A. Bonilla-Petriciolet and M. A. Montes-Morán, *Chem. Eng. J.*, **228**, 1098 (2013).
23. D. Mowla, G. Karimi and K. Salehi, *Chem. Eng. J.*, **218**, 116 (2013).
24. S. M. A. Guelli U. de Souza, L. C. Peruzzo and A. A. Ulson de Souza, *Appl. Math. Model.*, **32**, 1711 (2008).
25. S. Singha and U. Sarkar, *Korean J. Chem. Eng.*, **32**(1), 20 (2015).
26. R. M. Clark, *Environ. Sci. Technol.*, **21**, 573 (1987).
27. G. Bohart and E. Q. Adams, *J. Am. Chem. Soc.*, **42**, 523 (1920).
28. C. Faur, A. Cogunaud, G. Dreyfus and P. L. Cloirec, *Chem. Eng. J.*, **145**, 7 (2008).
29. Z. Aksu and F. Gönen, *Sep. Purif. Technol.*, **29**, 205 (2006).
30. A. Goshadrou and A. Moheb, *Desalination*, **269**, 170 (2011).
31. C. Escudero, J. Poch and I. Villaescusa, *Chem. Eng. J.*, **217**, 129 (2013).
32. Y. A. Alhamed, *J. Hazard. Mater.*, **170**, 763 (2009).
33. G. Vazquez, R. Alonso, S. Freire, J. G. Alvarez and G. Antorrena, *J. Hazard. Mater.*, **B 133**, 61 (2006).
34. J. J. Carberry and M. M. Wendel, *AIChE J.*, **9**, 129 (1963).
35. T. Sherwood and R. Pigford, Mass Transfer, McGraw-Hill, New York (1975).
36. W. E. Ranz and W. R. Marshall, *Chem. Eng. Prog.*, **48**, 173 (1952).
37. L. Lv, Y. Zhang, K. Wang, A. K. Ray and X. S. Zhao, *J. Colloid. Interf. Sci.*, **325**, 57 (2008).
38. J. M. Coulson and J. F. Richardson, Chemical Engineering, vol. 2, in: J. R. Buckhurst (Ed.), fifth ed., Particle Technology and Separation Processes, London, New York (2002).
39. D. M. Ruthven, *Principles of adsorption and adsorption processes*, Wiley, New York (1984).
40. Q. Yang, J. Zhang, Q. Yang, X. Tang, Y. Yu and G. Yang, *Trans. Tianjin Univ.*, **17**, 51 (2011).
41. L. Y. Tian, W. Ma and M. Han, *Chem. Eng. J.*, **156**, 134 (2010).
42. APHA, Standard Methods for the Examination of Water and Wastewater (21st edn.). In: Eaton AD, Clesceri LS, Rice EW, Greenberg AE and Franson MAH (eds.), American Public Health Association, American Water Works Association, Water Environment Federation, USA (2005).
43. I. Langmuir, *J. Am. Chem. Soc.*, **40**, 1361 (1918).
44. K. Kadirvelu and C. Namasivayam, *J. Membr. Sci.*, **165**, 159 (2000).

45. T. Lv, W. Ma, G. Xin, R. Wang, J. Xu, D. Liu and D. Pan, *J. Hazard. Mater.*, **237-238**, 121 (2012).
46. V. Srinivasa, P. Prasanna and K. Vishnu, *Solid State Sci.*, **10**, 260 (2008).
47. Q. Wang, Z. Wu, H. H. Tay, L. Chen, Y. Liu, J. Chang, Z. Zhong, J. Luo and A. Borgna, *Catal. Today*, **164**, 198 (2011).
48. V. Rives-Arnau, G. Munuera and J. M. Criado, *Spectrosc. Lett.*, **12**, 733 (1979).
49. F. M. Labajos, V. Rives and M. A. Ulibarri, *J. Mater. Sci.*, **27**, 1546 (1992).
50. K. Yang, L. Yan, Y. Yang, S. Yu, R. Shan, H. Yu, B. Zhu and B. Du, *Sep. Purif. Technol.*, **124**, 36 (2014).
51. F. Cavani, F. Trifirò and A. Vaccari, *Catal. Today*, **11**, 173 (1991).
52. K. Nakamoto, Infrared and Raman Spectra of Inorganic and Coordination Compounds (4th Ed.), John Wiley and Sons, New York, USA (1986).
53. Y. Li, B. Gao, T. Wu, D. Sun, X. Li, B. Wang and F. Lu, *Water Res.*, **43**, 3067 (2009).
54. K. V. Kumar and K. Porkodi, *J. Hazard. Mater.*, **146**, 214 (2007).
55. C. H. Giles, T. H. McEwans, S. N. Nakhwa and D. Smith, *J. Chem. Soc.*, **786**, 3973 (1960).
56. G. Mckay, H. S. Blair and J. K. Gardner, *J. Appl. Polym. Sci.*, **27**, 3043 (1982).
57. S. H. Lin and R. S. Juang, *J. Hazard. Mater.*, **B 113**, 195 (2004).
58. A. P. Lim and A. Z. Aris, *Biochem. Eng. J.*, **87**, 50 (2014).
59. M. Meng, Y. Feng, M. Zhang, Y. Liu, Y. Ji, J. Wang, Y. Wu and Y. Yan, *Chem. Eng. J.*, **225**, 331 (2013).
60. R. S. Juang and S. H. Lin, *J. Colloid Interface Sci.*, **269**, 46 (2004).
61. Y. Shao, H. Zhang and Y. Yan, *Chem. Eng. J.*, **225**, 488 (2013).
62. M. Auta and B. H. Hameed, *Chem. Eng. J.*, **237**, 352 (2014).
63. J. M. Chern and Y. W. Chien, *Water. Res.*, **36**, 647 (2002).